Eur. Phys. J. A **26**, 185–199 (2005)
DOI 10.1140/epja/i2005-10168-1

THE EUROPEAN PHYSICAL JOURNAL A

Single α-particle orbits and Bose-Einstein condensation in ^{12}C

T. Yamada[1,a] and P. Schuck[2]

[1] Laboratory of Physics, Kanto Gakuin University, Yokohama 236-8501, Japan
[2] Institute de Physique Nucléaire, F-91406 Orsay Cedex, France

Received: 1 October 2005 /
Published online: 13 December 2005 –
Communicated by G. Orlandini

Abstract. Bosonic properties of α particles such as single-α orbits and occupation numbers in $J^\pi = 0^+$, 2^+, 1^- and 3^- states of ^{12}C around the 3α threshold are investigated with the semi-microscopic 3α cluster model. As in other studies, we found that the 0_2^+ (2_2^+) state has dilute-3α-condensate–like structure in which the α particle is occupied in the single S (D) orbit with about 70% (80%) probability. The radial behaviors of the single-α orbits as well as the occupation numbers are discussed in detail in comparison with those for the 0_1^+ and 2_1^+ states together with the 1_1^- and 3_1^- states.

PACS. 21.10.Dr Binding energies and masses – 21.10.Gv Mass and neutron distributions – 21.60.Gx Cluster models – 03.75.Hh Static properties of condensates; thermodynamical, statistical and structural properties

1 Introduction

Four-nucleon correlations of the α-cluster type play an important role in nuclei. The microscopic α-cluster model [1–4] has succeeded in describing the structure of many states in light nuclei, in particular, around the threshold energy of breakup into constituent clusters. As for ^{12}C, detailed analyses were made by several authors with the microscopic 3α cluster model about 25 years ago. The 3α GCM (generator coordinate method) [5] and 3α RGM (resonating group method) [6] calculations showed that the second 0^+ state of ^{12}C ($E_x = 7.65$ MeV), located at $E_{3\alpha} = 0.38$ MeV above the 3α threshold, has a loosely coupled 3α structure, although the ground state is a shell-model–like compact state. On the other hand, special attention has been paid to an α-type condensation in symmetric nuclear matter, analogue to the Bose-Einstein condensation for finite number of dilute bosonic atoms such as ^{87}Rb or ^{23}Na at very low temperature where all atoms occupy the lowest S orbit [7]. Several authors [8,9] showed the possibility of such α-particle condensation in low-density nuclear matter, although the ordinary pairing correlation can prevail at higher densities. This result suggests that dilute α condensate states in finite nuclear system may exist in excited states as a weakly interacting gas of α particles.

Recently, a new α-cluster wave function was proposed which is of the $N\alpha$-particle condensate type [10]

$$|\Phi_{N\alpha}\rangle = (C_\alpha^+)^N|\mathrm{vac}\rangle, \tag{1}$$

$$\langle \boldsymbol{r}_1 \cdots \boldsymbol{r}_N|\Phi_{N\alpha}\rangle \propto \mathcal{A}\left\{e^{-\nu(\boldsymbol{r}_1^2+\cdots+\boldsymbol{r}_N^2)}\phi(\alpha_1)\cdots\phi(\alpha_N)\right\}, \tag{2}$$

where C_α^+ is the α-particle creation operator, $\phi(\alpha)$ denotes the internal wave function of the α cluster, $\boldsymbol{r}_i$ is the center-of-mass coordinate of the i-th α cluster, and $\mathcal{A}$ presents the antisymmetrizer among the nucleons belonging to different α clusters. The important characteristic of the wave function is that the center-of-mass motion of each α cluster is of S-wave type. Applications of the condensate-type wave function to ^{12}C and ^{16}O [10] indicated that the second 0^+ state of ^{12}C ($E_x = 7.65$ MeV) and fifth 0^+ state of ^{16}O ($E_x = 14.0$ MeV), around the 3α and 4α threshold, respectively, are conjectured to be dilute $N\alpha$ condensate states, which are quite similar to the Bose-Einstein condensation of bosonic atoms at very low temperature. The calculated nuclear radii for both of those states are about 4 fm, significantly larger than that for the ground state (about 2.5–2.7 fm). As for ^{12}C, a detailed analysis with a deformed alpha condensate wave function, slightly different from the spherical one in eq. (2), was performed to investigate the structure of the 0_1^+ and 0_2^+ states [11]. It was found that each of the 0_2^+ wave functions obtained by the 3α GCM and RGM calculations has a large squared overlap value of more than 90% with the single 3α condensate wave function.

[a] e-mail: yamada@kanto-gakuin.ac.jp

The above-mentioned results for ^{12}C and ^{16}O lead us to the further intriguing issue that dilute α-cluster states with $J^\pi = 0^+$ near the $N\alpha$ threshold may exist in other heavier $4N$ self-conjugate nuclei. The Gross-Pitaevskii equation approach [12] is useful to explore such dilute multi-α systems, because this equation [13], based on mean-field theory, has succeeded in describing the structure of the Bose-Einstein condensation for dilute neutral atomic systems, for example, ^{87}Rb or ^{23}Na, at very low temperature, trapped by an external magnetic field [7]. The present authors [12] applied the Gross-Pitaevskii equation to self-conjugate $4N$ nuclei. They found that 1) there exists a critical number of α bosons that the dilute $N\alpha$ system can sustain as a self-bound nucleus, and 2) the Coulomb potential barrier plays an important role to confine such dilute $N\alpha$-particle condensate states.

It is interesting to explore also the possibility of the α condensate states with non-zero angular momentum in ^{12}C. The old theoretical calculations based on the microscopic 3α cluster model [4–6] suggested the existence of a 2_2^+ state of ^{12}C at around $E_{3\alpha} \sim 3$ MeV above the 3α threshold, the structure of which is similar to the 0_2^+ state except for the angular momentum. Quite recently the 2_2^+ state was observed at $E_{3\alpha} = 2.6 \pm 0.3$ MeV with the alpha decay width $\Gamma_\alpha = 1.0 \pm 0.3$ MeV [14]. The α-condensate–type wave function with axial deformation [15] was applied to study the structure of the 2_2^+ state with help of the method of ACCC (analytic continuation in the coupling constant) [16]. They found that the 2_2^+ state has a large overlap with the single condensate wave function of 3α gas-like structure, the squared value of which amounts to about 88%. This result implies that the 2_2^+ state has a similar structure as the 0_2^+ state, namely, an excited state of the dilute 3α condensation.

Here, it is an intriguing problem to discuss whether the 0_2^+ and 2_2^+ states of ^{12}C are *ideal* dilute α condensates or not. The condensate-type α-cluster wave function in eq. (2) has succeeded in describing the 0_2^+ state of ^{12}C. This result, however, does not necessarily mean that the 0_2^+ state of ^{12}C is an ideal α condensate state. If the 0_2^+ state of ^{12}C is an ideal dilute α condensate, the single α-particle orbit in the state should be of the zero-node long-ranged S-wave type with an occupation probability of 100%, as suggested from the Gross-Pitaevskii equation approach [12]. The antisymmetrizer $\mathcal{A}$ in eq. (2) generally perturbs the single α motion in the nucleus, and one should remember that the condensate-type wave function can also describe the shell-model–like compact structure of the ground state of ^{12}C. The effect of the antisymmetrizer should have a close relation to the rms radius of the nucleus or the distance between 2α clusters in a nucleus. The ideal 3α condensate state is expected to be realized if the distance between two arbitrary α clusters is large enough so that the effect of the antisymmetrizer can be neglected. The calculated nuclear radius for the 0_2^+ state of ^{12}C, about 4 fm [10], suggests that the action of the antisymmetrizer is weakened significantly in that state. In order to give more decisive theoretical evidence that the 0_2^+ state of ^{12}C as well as the 2_2^+ state has dilute 3α condensation structure, it is needed to study quantitatively the bosonic properties such as single α-particle orbits and corresponding occupation probabilities, starting from the microscopic wave function.

The first attempt to derive the α-boson properties for 0^+ states in ^{12}C from a microscopic model was performed in ref. [17], where the 3α RGM equation was solved in terms of the correlated Gaussian basis with the stochastic variational method. Although the authors formulated a derivation of the 3α boson wave function starting from the microscopic 3α wave function, the α bosonic properties of ^{12}C were studied not with the 3α bosonic wave function but with the normalized spectroscopic amplitude, because the derivation of the 3α boson wave function is numerically difficult due to the non-local properties of the norm kernel. Although the normalized spectroscopic amplitude seems to be a good approximation for the boson wave function in the region where the effect of the antisymmetrizer is negligible, the approximation becomes worse when the spatial overlap of the 3α clusters becomes larger. It is desirable to investigate quantitatively how good that approximation is for the 0_2^+ state within their framework.

The purposes in the present paper are twofold. First, we study the bosonic properties such as single α-particle orbits and their occupation probabilities for the 0^+ and 2^+ states in ^{12}C with direct use of the wave function obtained by the 3α OCM (orthogonality condition model) [18]. The OCM is a semi-microscopic model and a simple version of the RGM, taking into account properly the antisymmetrization among nucleons, which successfully describes the structure of ^{12}C [4,19–23]. The second purpose is to explore the possibility of the dilute 3α condensation with *negative* parity within the present framework. The 3_1^- (1_1^-) state of ^{12}C at $E_{3\alpha} = 2.37$ (3.57) MeV above the 3α threshold appears at the same energy region as that for the 0_2^+ ($E_x = 0.38$ MeV) and 2_2^+ (2.6 MeV) states. According to the old theoretical study based on the 3α GCM and RGM calculations [5,6], the nuclear radius of the 3^- state is intermediate between a compact shell-model–like state (0_1^+) and a loosely coupled 3α cluster state (0_2^+), while the 1^- state has a radius only a little smaller than that of the 0_2^+ state. Thus, it is quite interesting to study the bosonic properties for the negative-parity states, as well.

In sect. 2, we formulate the $N\alpha$ OCM equation with emphasis on a close relation with the equation of motion of $N\alpha$ bosons, the wave function of which is mapped from the microscopic $N\alpha$ wave function within the framework of the resonating group method (RGM). The $N\alpha$ OCM wave function has bosonic properties. The 3α OCM equation is solved properly with modern numerical techniques. The calculated single α-particle orbits and occupation probabilities in ^{12}C are discussed in sect. 3. Finally, we give the summary in sect. 4.

2 Formulation

The $N\alpha$ OCM equation is given as an approximation of the equation of motion of the $N\alpha$ bosons, the wave function of which is mapped from the microscopic $N\alpha$ wave

function within the framework of the resonating group method (RGM). We first will briefly see a relationship between the equation of motion of the $N\alpha$ boson and the $N\alpha$ OCM equation, and then, formulate the evaluation of the single-α orbits and occupation numbers from the $N\alpha$ OCM wave function together with other physical quantities. Finally, we give an outline of how to solve the 3α OCM equation for ^{12}C with a phenomenological α-α potential.

2.1 Nα orthogonality condition model (OCM) with bosonic properties

An $N\alpha$ boson wave function $\Phi_J^{(B)}$ corresponding to the microscopic (fermionic) $N\alpha$ cluster model wave function is provided within the RGM framework [24,17],

$$\Phi_J^{(B)}(\boldsymbol{r}) = \mathcal{N}^{1/2}\chi_J = \int \mathrm{d}\boldsymbol{r}' N^{1/2}(\boldsymbol{r},\boldsymbol{r}')\chi_J(\boldsymbol{r}'), \tag{3}$$

where χ_J represents the relative wave function with a set of the relative (Jacobi) coordinates, $\boldsymbol{r} = \{\boldsymbol{r}_1, \boldsymbol{r}_2, \cdots, \boldsymbol{r}_{N-1}\}$, with respect to the c.m. of α clusters, and J denotes the total angular momentum of the $N\alpha$ system. The square-root matrix $N^{1/2}(\boldsymbol{r},\boldsymbol{r}')$ is relevant to the norm kernel of the $N\alpha$ RGM wave function, $\Psi^{(F)}(\boldsymbol{a}) = \mathcal{A}\left\{\prod_{i=1}^{N}\phi_{\alpha_i}^{(\mathrm{int})}\prod_{j=1}^{N-1}\delta(\boldsymbol{r}_j - \boldsymbol{a}_j)\right\}$, where $\phi_\alpha^{(\mathrm{int})}$ denotes the intrinsic wave function of the α particle with the simple $(0s)^4$ shell model configuration ($\mathcal{A}$ is the anti-symmetrization operator among $4N$ nucleons). It is noted that $\Phi_J^{(B)}(\boldsymbol{r})$ has only the Jacobi coordinates of the $N\alpha$ system and the internal coordinates in the α cluster are integrated out completely. The equation of motion for $\Phi_J^{(B)}(\boldsymbol{r})$ is given as

$$\left(\mathcal{N}^{-1/2}\mathcal{H}\mathcal{N}^{-1/2} - E\right)\Phi_J^{(B)} = 0, \tag{4}$$

where $\mathcal{H}$ denotes the Hamiltonian kernel of the $N\alpha$ RGM wave function $\Psi^{(F)}$, and $\mathcal{N}^{-1/2}\mathcal{H}\mathcal{N}^{-1/2}$ can be interpreted as the $N\alpha$ boson Hamiltonian.

The boson wave function has the following properties: 1) $\Phi_J^{(B)}$ is totally symmetric for any 2α-particle exchange, 2) $\Phi_J^{(B)}$ satisfies the equation motion in eq. (4), and 3) $\Phi_J^{(B)}$ is orthogonal to the Pauli-forbidden state $u_F(\boldsymbol{r})$, which satisfies the condition $\mathcal{A}\left\{\prod_{i=1}^{N}\phi_{\alpha_i}^{(\mathrm{int})}u_F\right\} = 0$. In order to obtain the boson wave function, we need to solve the equation of motion of the bosons in eq. (4). Solving the boson equation, however, is difficult in general even for the 3α case. Thus, it is requested to use more feasible frameworks for the study of the bosonic properties and the amount of α condensation for the $N\alpha$ system. In the present study, we take the orthogonality condition model (OCM) [18] as one of the more feasible frameworks. The OCM scheme, which is an approximation to the RGM, is known to describe nicely the structure of low-lying states in light nuclei [4,18–20,23]. The essential properties of the $N\alpha$ boson wave function $\Phi_J^{(B)}$, as mentioned above, can be taken into account in OCM in a simple manner. We will demonstrate this briefly.

In OCM, the α cluster is treated as a point-like particle. We approximate the $N\alpha$ boson Hamiltonian (non-local) in eq. (4) by an effective (local) one $H^{(\mathrm{OCM})}$,

$$\mathcal{N}^{-1/2}\mathcal{H}\mathcal{N}^{-1/2} \sim H^{(\mathrm{OCM})}, \tag{5}$$

$$H^{(\mathrm{OCM})} \equiv \sum_{i=1}^{N} T_i - T_{\mathrm{cm}} + \sum_{i<j=1}^{N} V_{2\alpha}^{\mathrm{eff}}(i,j) + \sum_{i<j<k=1}^{N} V_{3\alpha}^{\mathrm{eff}}(i,j,k), \tag{6}$$

where T_i denotes the kinetic energy of the i-th α cluster, and the center-of-mass kinetic energy T_{cm} is subtracted from the Hamiltonian. The effective 2α and 3α potentials are presented as $V_{2\alpha}^{\mathrm{eff}}$ and $V_{3\alpha}^{\mathrm{eff}}$, respectively. Then, the equation of the relative motions for the $N\alpha$ particles with $H^{(\mathrm{OCM})}$, called the OCM equation, is expressed as

$$\left\{H^{(\mathrm{OCM})} - E\right\}\Phi_J = 0, \tag{7}$$

$$\langle u_F \mid \Phi_J\rangle = 0, \tag{8}$$

where u_F denotes the Pauli-forbidden state of the $N\alpha$ system as mentioned above. The bosonic property of the wave function Φ_J can be taken into account by symmetrizing the wave function with respect to any 2α-particle exchange,

$$\Phi_J = \mathcal{S}\Phi_J(1,2,\cdots,N), \tag{9}$$

where $\mathcal{S}$ denotes the symmetrization operator, $\mathcal{S} = (1/\sqrt{N!})\sum_{\mathcal{P}}\mathcal{P}$, where the sum runs over all permutations $\mathcal{P}$ for the $N\alpha$ particles. It is noted that the complete overlapped state of the 3α particles is forbidden within the present framework because of the Pauli-blocking effect in eq. (8), although we take into account the bosonic statistics for the constituent α particles. In the next section, we will demonstrate i) how to solve the OCM equation and ii) what kind of effective α-α potential we should choose in $H^{(\mathrm{OCM})}$ for the 3α case of ^{12}C.

Here, it is useful to define various quantities characterizing the structure of the $N\alpha$ system with use of the $N\alpha$ boson wave function Φ_J obtained by solving the OCM equation in eqs. (7) and (8). The single α-particle density is defined as

$$\rho(\boldsymbol{r}) = \langle\Phi_J \mid \sum_{i=1}^{N}\delta(\boldsymbol{r} - \boldsymbol{r}_i^{(\mathrm{cm})}) \mid \Phi_J\rangle, \tag{10}$$

where $\boldsymbol{r}_i^{(\mathrm{cm})}$ is the coordinate of the i-th α particle measured from the center-of-mass coordinate of the total system. The nuclear root-mean-square radius is given as

$$\sqrt{\langle r_N^2\rangle} = \sqrt{\langle r_\alpha^2\rangle + 1.71^2}, \tag{11}$$

$$\sqrt{\langle r_\alpha^2\rangle} = \int \mathrm{d}\boldsymbol{r} r^2\rho(\boldsymbol{r}), \tag{12}$$

where we take into account the finite-size effect of the α particle. The correlation functions with respect to the α-α relative coordinate $\boldsymbol{r}_{\alpha\alpha}$ as well as the relative coordinate between one of the α particles and the remaining $(N-1)\alpha$ system $\boldsymbol{r}_{\alpha\text{-}(N-1)\alpha}$ are given as

$$f_{\alpha\alpha}(r) = \langle \Phi_J \mid \delta(\boldsymbol{r} - \boldsymbol{r}_{\alpha\alpha}) \mid \Phi_J \rangle, \tag{13}$$

$$f_{\alpha\text{-}(N-1)\alpha}(r) = \langle \Phi_J \mid \delta(\boldsymbol{r} - \boldsymbol{r}_{\alpha\text{-}(N-1)\alpha}) \mid \Phi_J \rangle, \tag{14}$$

where the way of choosing the coordinates, $\boldsymbol{r}_{\alpha\alpha}$ and $\boldsymbol{r}_{\alpha\text{-}(N-1)\alpha}$, is arbitrary in the set of Jacobi coordinates of the $N\alpha$ particles because of the totally symmetrization for Φ_J. The root-mean-square (rms) distances with respect to $\boldsymbol{r}_{\alpha\alpha}$ and $\boldsymbol{r}_{\alpha-(N-1)\alpha}$ are, respectively, given by

$$\sqrt{\langle r^2_{\alpha\alpha} \rangle} = \left[\langle \Phi_J \mid \boldsymbol{r}^2_{\alpha\alpha} \mid \Phi_J \rangle \right]^{1/2}, \tag{15}$$

$$\sqrt{\langle r^2_{\alpha\text{-}(N-1)\alpha} \rangle} = \left[\langle \Phi_J \mid \boldsymbol{r}^2_{\alpha\text{-}(N-1)\alpha} \mid \Phi_J \rangle \right]^{1/2}. \tag{16}$$

The reduced width amplitude for the α-$(N-1)\alpha$ part is defined as

$$\mathcal{Y}_{\ell L J}(r) = r \times \langle [Y_L(\boldsymbol{r}) \phi_\ell \left((N-1)\alpha\right)]_J \mid \Phi_J \rangle \,, \tag{17}$$

where $\boldsymbol{r}$ denotes the relative coordinate between the α particle and the $(N-1)\alpha$ nucleus, and $\phi_\ell \left((N-1)\alpha\right)$ represents the wave function of the $(N-1)\alpha$ nucleus with total angular momentum ℓ which is obtained by solving the OCM equation for the $(N-1)\alpha$ system. The integration in eq. (17) is done over all of the relative (Jacobi) coordinates for the $N\alpha$ system except for the radial part of $\boldsymbol{r}$.

In order to discuss the bosonic properties such as the degree of α condensation in a nucleus, it is needed to extract information on the single α-particle orbits and their occupation probabilities in the nucleus from the total wave function Φ_J. The one-particle density matrix for the $N\alpha$ system is very useful for this [17]. Defining the one-particle density operator as

$$\mathcal{D}(\boldsymbol{r}, \boldsymbol{r}') = \sum_{i=1}^{N} \mid \delta(\boldsymbol{r}_i^{(\mathrm{cm})} - \boldsymbol{r}') \rangle \langle \delta(\boldsymbol{r}_i^{(\mathrm{cm})} - \boldsymbol{r}) \mid, \tag{18}$$

then, the single α-particle density matrix is given as

$$\rho(\boldsymbol{r}, \boldsymbol{r}') = \langle \Phi_J \mid \mathcal{D}(\boldsymbol{r}, \boldsymbol{r}') \mid \Phi_J \rangle, \tag{19}$$

$$= N \times \langle \Phi_J \mid \delta(\boldsymbol{r}_1^{(\mathrm{cm})} - \boldsymbol{r}') \rangle \langle \delta(\boldsymbol{r}_1^{(\mathrm{cm})} - \boldsymbol{r}) \mid \Phi_J \rangle, \tag{20}$$

where $\boldsymbol{r}_i^{(\mathrm{cm})}$ is the same as that in eq. (10). It is noted that the diagonal matrix element reduces to the single α-particle density in eq. (10): $\rho(\boldsymbol{r}, \boldsymbol{r}' = \boldsymbol{r}) = \rho(\boldsymbol{r})$. The single α-particle orbit and its occupation number in the nucleus can be evaluated by solving the eigenvalue equation of the one-particle density matrix

$$\int \mathrm{d}\boldsymbol{r}' \rho(\boldsymbol{r}, \boldsymbol{r}') \varphi_\mu(\boldsymbol{r}') = \mu \varphi_\mu(\boldsymbol{r}), \tag{21}$$

where the eigenvalue μ presents the occupation number. The eigenfunction φ_μ denotes the single-α orbital wave function in a nucleus with the argument of the intrinsic coordinate ($\boldsymbol{r}_\alpha^{(\mathrm{cm})}$) of an arbitrary α particle in a nucleus measured from the center-of-mass coordinate. The ratio μ/N represents the occupation probability of an α particle in the orbit φ_μ. The spectrum of the occupation probabilities offers important information about the occupancy of the single α-particle orbit in a nucleus. If each of the $N\alpha$ particles in an $N\alpha$-boson state is occupied by only one orbit, the occupation probability for this orbit becomes 100%.

The ^{8}Be (2α) system is a good example to demonstrate the characteristic of the single-α orbital wave function. From the definition of eqs. (20) and (21), the L_α-wave single-α orbit in the $^8\mathrm{Be}(J^\pi)$ state corresponds to the relative wave function (which is obtained by solving the 2α OCM equation with J (= L_α) in eqs. (7) and (8)), scaling to 1/2 with respect to the relative coordinate between the 2α clusters. Then, the occupation probability becomes exactly (mathematically) 100% for any L_α-value.

The radial behavior of the L_α-wave single-α orbit, $\varphi_\mu(r_\alpha^{(\mathrm{cm})})$, in eq. (21) generally has a close relationship with that of the reduced width amplitude, $\mathcal{Y}_{\ell L J}(r_{\alpha\text{-}(N-1)\alpha})$, in eq. (17). This is due to the fact that both represent the behavior of the single α-particle motion in a nucleus in which all degrees of freedom of the other α particles are integrated out, and $\boldsymbol{r}_\alpha^{(\mathrm{cm})}$ is given as $\boldsymbol{r}_\alpha^{(\mathrm{cm})} = \frac{N-1}{N} \times \boldsymbol{r}_{\alpha\text{-}(N-1)\alpha}$.

The momentum distribution of the single α particle is also helpful for the study of α condensation in a nucleus [17]. It is defined as a double Fourier transformation of the one-particle density matrix

$$\rho(k) = \int \mathrm{d}\boldsymbol{r}' \mathrm{d}\boldsymbol{r} \frac{e^{i\boldsymbol{k}\cdot\boldsymbol{r}'}}{(2\pi)^{3/2}} \rho(\boldsymbol{r}, \boldsymbol{r}') \frac{e^{-i\boldsymbol{k}\cdot\boldsymbol{r}}}{(2\pi)^{3/2}}, \tag{22}$$

$$\int \mathrm{d}\boldsymbol{k} \rho(k) = 1. \tag{23}$$

It is reminded that $\rho(k)$ would have a δ-function–like peak around $k = 0$ for an ideal dilute condensed state in homogeneous infinite matter.

2.2 3α OCM for ^{12}C

In the previous section, we outlined the $N\alpha$ orthogonality condition model (OCM) and discussed how to extract the properties and the amount of α condensation in the $N\alpha$ system. Here, we will apply the OCM framework to the 3α system of ^{12}C.

The total wave function of ^{12}C (the total angular momentum J) within the frame of the 3α OCM is presented as

$$\Phi_J(^{12}\mathrm{C}) = \Phi_J^{(12,3)} + \Phi_J^{(23,1)} + \Phi_J^{(31,2)}, \tag{24}$$

where $\Phi_J^{(12,3)}$ denotes the relative wave function of the 3α system with the Jacobi-coordinate system shown in fig. 1(a), and other notations are self-explanatory. In the

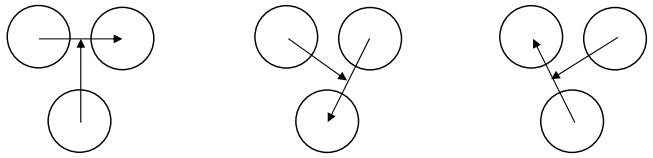

Fig. 1. Jacobian-coordinate systems for the 3α model of ^{12}C. The three Jacobian coordinates, (a), (b) and (c), correspond, respectively, to the 3α relative wave functions, $\Phi^{3\alpha}_J(12,3)$, $\Phi^{3\alpha}_J(23,1)$ and $\Phi^{3\alpha}_J(31,2)$ in eq. (24).

present study, $\Phi_J(^{12}\mathrm{C})$ is expanded in terms of the Gaussian basis [25],

$$\Phi_J(^{12}\mathrm{C}) = \sum_c \sum_{\nu,\mu} A_c(\nu,\mu)\Phi^{3\alpha}_c(\nu,\mu), \tag{25}$$

$$\Phi^{3\alpha}_c(\nu,\mu) = \Phi^{(12,3)}_c(\nu,\mu) + \Phi^{(23,1)}_c(\nu,\mu) + \Phi^{(31,2)}_c(\nu,\mu), \tag{26}$$

$$\Phi^{(ij,k)}_c(\nu,\mu) = \left[\varphi_\ell(\boldsymbol{r}_{ij},\nu)\varphi_L(\boldsymbol{r}_k,\mu)\right]_J, \tag{27}$$

$$\varphi_\ell(\boldsymbol{r},\nu) = N_\ell(\nu) r^\ell \exp(-\nu r^2) Y_\ell(\hat{\boldsymbol{r}}), \tag{28}$$

where N_ℓ is the normalization factor, and $\boldsymbol{r}_{ij}$ ($\boldsymbol{r}_k$) denotes the relative coordinate between the i- and j-th α particle (the k-th α particle and the center-of-mass coordinate of the i-th and j-th α particle). The angular momentum channel is presented as $c = (\ell, L)_J$, where ℓ (L) denotes the relative orbital angular momentum between 2α clusters (the center of mass for the 2α clusters and the third α). The Gaussian parameter ν is taken to be of geometrical progression,

$$\nu_n = 1/b_n^2, \qquad b_n = b_{\min} a^{n-1}, \qquad n = 1 \sim n_{\max}. \tag{29}$$

It is noted that the prescription is found to be very useful in optimizing the ranges with a small number of free parameters with high accuracy [25].

The total Hamiltonian for the 3α system is presented as

$$\mathcal{H} = \sum_{i=1}^{3} T_i - T_{\mathrm{cm}} + \sum_{i<j=1}^{3} \left[V_{2\alpha}(r_{ij}) + V^{\mathrm{Coul}}_{2\alpha}(r_{ij})\right] + V_{3\alpha}(r_{12}, r_{23}, r_{31}) + V_{\mathrm{Pauli}}, \tag{30}$$

where T_i, $V_{2\alpha}$ and $V_{3\alpha}$ stand for the kinetic energy operator for the i-th α particle, phenomenological 2α and 3α potentials, respectively, and $V^{\mathrm{Coul}}_{2\alpha}$ is the Coulomb potential between 2α particles. The center-of-mass kinetic energy is subtracted from the Hamiltonian. The Pauli-blocking operator V_{Pauli} [26] is represented as

$$V_{\mathrm{Pauli}} = \lim_{\lambda\to\infty} \lambda \hat{O}_{\mathrm{Pauli}}, \tag{31}$$

$$\hat{O}_{\mathrm{Pauli}} = \sum_{2n+\ell<4,\ell=\mathrm{even}} \sum_{(ij)=(12),(23),(31)} |u_{n\ell}(\boldsymbol{r}_{ij})\rangle\langle u_{n\ell}(\boldsymbol{r}_{ij})|, \tag{32}$$

which removes the Pauli-forbidden states, u_{00}, u_{10} and u_{20}, between any two α particles from the 3α model space. The Gaussian size parameter of the nucleon ($0s$) orbit in the α cluster is taken to be $b_N = 1.358$ fm, which reproduces the size of the α particle in free space. In the present study, we take the harmonic-oscillator wave functions as the Pauli-forbidden states. The eigenenergy E of ^{12}C and coefficients A_c in eq. (25) are obtained in terms of the variational principle,

$$\delta\left[\langle\Phi_J \mid \mathcal{H} - E \mid \Phi_J\rangle\right] = 0. \tag{33}$$

We use an effective 2α potential which reproduces the observed α-α scattering phase shifts (S, D and G waves) and the resonant ground-state energy within the 2α OCM framework. The effective 2α potential and Coulomb potential, $V_{2\alpha}$ and $V^{\mathrm{Coul}}_{2\alpha}$, are constructed with the folding procedure, where we fold the modified Hasegawa-Nagata effective NN interaction (MHN) and the pp Coulomb potential with the α-cluster density. Also the strength of the second-range triplet-odd part in MHN is modified so as to reproduce the 2α scattering phase shifts.

Only using the effective 2α potential leads to a significant overbinding energy for the ground state of ^{12}C within the frame of the 3α OCM. Thus, we introduce an effective, repulsive, 3α potential, $V_{3\alpha}$, in addition to the 2α potential,

$$V_{3\alpha} = V_0 \exp\left[-\beta\left(\boldsymbol{r}^2_{12} + \boldsymbol{r}^2_{23} + \boldsymbol{r}^2_{31}\right)\right], \tag{34}$$

where $\boldsymbol{r}_{ij}$ denotes the relative coordinate between the i- and j-th α particles, and V_0 and β are taken to be $V_0 = 87.5$ MeV and $\beta = 0.15$ fm^{-2}. Including the 3α potential, the energy of the ground state of ^{12}C is reproduced with respect to the 3α threshold, together with the nuclear radius (see sect. 3).

Single-α orbits and corresponding occupation probabilities for 0^+, 2^+, 1^-, and 3^- states of ^{12}C are investigated by solving the eigenvalue equation of the single α-particle density matrix in eqs. (20) and (21) (see sect. 2.2). They will lead to a deep understanding about the structure of ^{12}C.

In the present investigation, we make a further structure study for the 0^+ states of ^{12}C, because they have very intriguing features. According to ref. [10], the 0^+_1 state has a compact shell-model–like state, while the 0^+_2 one is conjectured to have a dilute 3α condensate structure, the nuclear radius of which is 4.3 fm, much larger than that of the ground 0^+_1 state (2.48 fm). Thus, it is interesting to see in detail the structure change of the 0^+ state of ^{12}C by taking the nuclear radius as a parameter. We investigate the dependence of the occupation probabilities and radial behaviors of the single α-particle orbits in the 0^+ state on its rms radius within the 3α OCM framework. The results will give us helpful understanding about the structure of ^{12}C. The procedure is formulated hereafter.

First, we consider a Pauli-principle–respecting 3α OCM basis wave function. For the purpose, the eigenvalue problem for the Pauli operator in eq. (32) is solved to obtain the Pauli-forbidden state in the 3α OCM model space

$$\hat{O}_{\mathrm{Pauli}}|G^{3\alpha}_P\rangle = \lambda_P|G^{3\alpha}_P\rangle, \tag{35}$$

where λ_P denotes the eigenvalue for the eigenfunction $|G_P^{3\alpha}\rangle$. The Pauli operator, then, is expressed as

$$\hat{O}_{\rm Pauli} = \sum_P |G_P^{3\alpha}\rangle \lambda_P \langle G_P^{3\alpha}|. \tag{36}$$

If λ_P is non-zero, its eigenfunction corresponds to the Pauli-forbidden state. In the present study, the eigenvalue problem is solved with use of the 3α OCM basis in eq. (26). Then, the Pauli-principle–respecting OCM basis wave function is given by

$$\tilde{\Phi}_c^{3\alpha}(\nu,\mu) = N_c(\nu,\mu)\Big[\Phi_c^{3\alpha}(\nu,\mu) - \sum_{\lambda_P\neq 0} |G_P^{3\alpha}\rangle\langle G_P^{3\alpha}|\Phi_c^{3\alpha}(\nu,\mu)\rangle\Big], \tag{37}$$

where N_c denotes the normalization factor with the angular momentum channel $c = (\ell, L)_J$, and $\Phi_c^{3\alpha}(\nu,\mu)$ is given in eq. (26). The energy of the 3α system, then, is given by

$$E_{3\alpha}(\nu,\mu) = \left\langle \tilde{\Phi}_c^{3\alpha}(\nu,\mu)|\tilde{\mathcal{H}}|\tilde{\Phi}_c^{3\alpha}(\nu,\mu)\right\rangle. \tag{38}$$

where $\tilde{\mathcal{H}}$ denotes the total Hamiltonian of the 3α system in which we subtract the Pauli-blocking operator $V_{\rm Pauli}$ from the 3α OCM Hamiltonian $\mathcal{H}$ in eq. (30). Applying the wave function in eq. (37) to eqs. (20) and (21), we can study the dependence of the occupancy of the single α-particle orbits in the 0^+ state of ^{12}C on its nuclear radius by choosing the parameter values, ν and μ, so as to reproduce a given nuclear radius. In the present study, we consider only the case of the equilateral triangle configuration of the 3α clusters (see sect. 3.5).

3 Results and discussion

3.1 0_1^+ and 0_2^+ states

Table 1 presents the results for the energy, measured from the 3α threshold, and nuclear radii for the ground (0_1^+) and excited states (0_2^+) of ^{12}C. The energy for the ground state is reproduced well, and the corresponding nuclear radius, 2.44 fm, is in good agreement with the experimental charge radius (2.4829 ± 0.019 fm) with an error of about 2%. On the other hand, the rms distance between 2α clusters in the 0_1^+ state is $\sqrt{\langle r^2\rangle_{\alpha\alpha}} = 3.02$ fm (see table 1), which is larger than that between the center of mass of the 2α clusters and the third α cluster, $\sqrt{\langle r^2\rangle_{\alpha\text{-}2\alpha}} = 2.61$ fm. Then, the square of the ratio, $\left[\sqrt{\langle r^2\rangle_{\alpha\text{-}2\alpha}}/\sqrt{\langle r^2\rangle_{\alpha\alpha}}\right]^2$, is about 3/4. The results mean that the ground state has an equilateral-triangle–like intrinsic shape. Figure 2 shows the density distribution of the α particle for the 0_1^+ state of ^{12}C. We see a prominent peak at $r \sim 2$ fm, which demonstrates clearly the shell-model–like compact structure of the ground state of ^{12}C.

Table 1. Calculated energies ($E_{3\alpha}$) and nuclear radii ($\sqrt{\langle r_N^2\rangle}$) for the 0^+, 2^+, 3^- and 1^- states of ^{12}C together with the α-α and α-2α rms distances ($\sqrt{\langle r_{\alpha\alpha}^2\rangle}$ and $\sqrt{\langle r_{\alpha\text{-}2\alpha}^2\rangle}$). The energy $E_{3\alpha}$ is the one measured from the 3α threshold. The values in parenthesis denote the experimental ones. All energies and nuclear radii (rms distances) are given in units of MeV and fm, respectively.

J^π	$E_{3\alpha}^{\rm cal}$	$(E_{3\alpha}^{\rm exp})$	$\sqrt{\langle r_N^2\rangle}$	$\sqrt{\langle r_{\alpha\alpha}^2\rangle}$	$\sqrt{\langle r_{\alpha\text{-}2\alpha}^2\rangle}$
0_1^+	-7.27	(-7.27)	2.44	3.02	2.61
0_2^+	0.85	(0.38)	4.31	6.84	5.93
2_1^+	-5.28	(-2.83)	2.45	2.94	2.55
2_2^+	$2.43^{(a)}$	(2.6)	$6.12^{(a)}$	10.2	8.80
3_1^-	1.52	(2.37)	2.96	4.10	3.56
1_1^-	3.11	(3.57)	3.32	4.87	4.23

(^{a}) According to the complex-scaling method, the resonant energy and width of the 2_2^+ state are $E_{3\alpha} = 2.3$ MeV and $\Gamma = 1.0$ MeV, respectively, with $\sqrt{\langle r_N^2\rangle} = 4.3$ fm. See text.

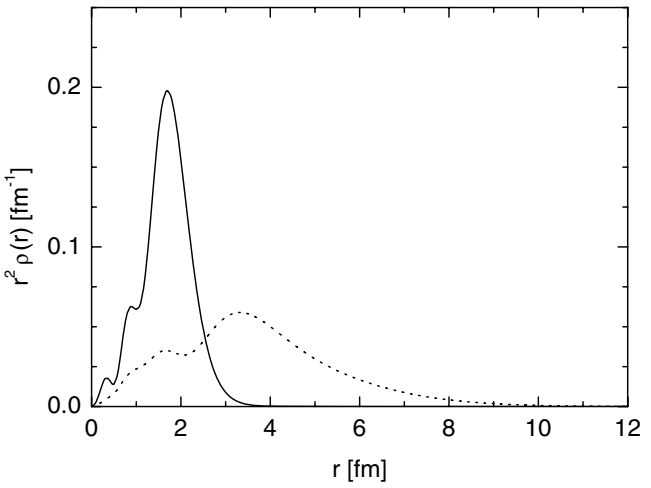

Fig. 2. Density distribution of the α particle for the 0_1^+ (solid line) and 0_2^+ (dotted line) states.

As for the 0_2^+ state, the energy measured from the 3α threshold is $E_{3\alpha} = 0.86$ MeV ($E_x = 8.13$ MeV), which agrees well with the experimental data $E_{3\alpha}^{\rm exp} = 0.38$ MeV ($E_x^{\rm exp} = 7.65$ MeV). The calculated nuclear radius for the 0_2^+ state is as large as 4.31 fm (see table 1). This means that the state has a dilute 3α structure, although our nuclear radius is a little larger than that in ref. [10]. The density distribution of the α particle for the 0_2^+ state is illustrated in fig. 2. In comparison with that for the ground state, we can easily recognize the dilute structure of the 0_2^+ state, which is in contrast with the compact structure of the ground state.

The difference between the structures of the 0_1^+ and 0_2^+ states can be also seen in the radial behavior of the correlation functions, $f_{\alpha\alpha}$ and $f_{\alpha\text{-}2\alpha}$, with respect to the α-α and α-2α relative coordinates, respectively, of eqs. (13) and (14). They are illustrated in fig. 3. Reflecting the compact

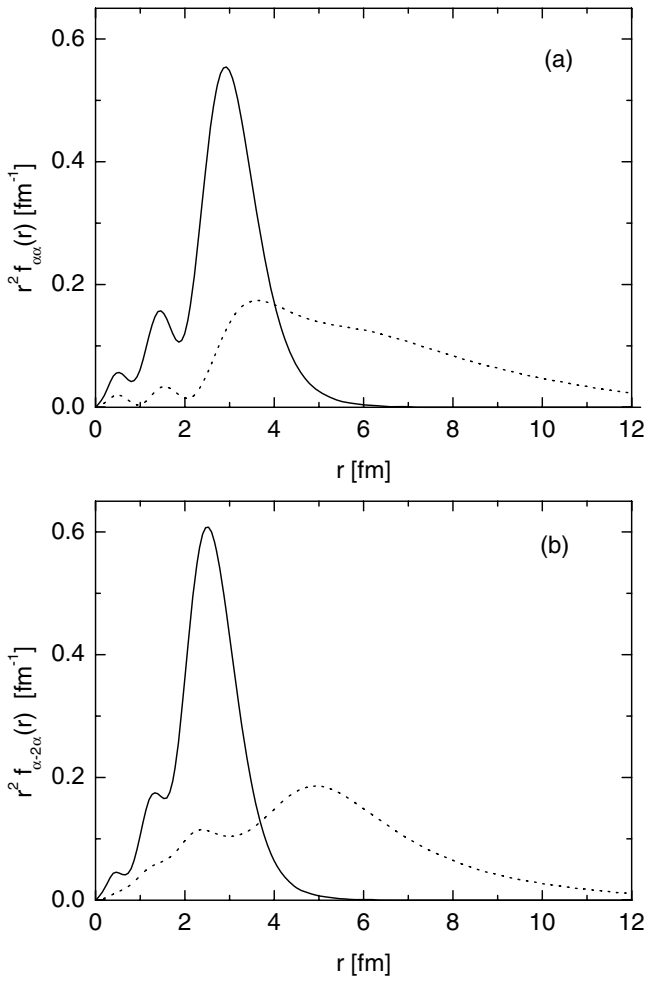

Fig. 3. Correlation functions, (a) $f_{\alpha\alpha}$ and (b) $f_{\alpha\text{-}2\alpha}$, for the 0_1^+ (solid line) and 0_2^+ (dotted line) states.

structure of the 0_1^+ state, both $f_{\alpha\alpha}$ and $f_{\alpha\text{-}2\alpha}$ have prominent peaks at $r \sim 2.6$ fm and 2.5 fm, respectively, and extend to $r \sim 5$ fm, while those for the 0_2^+ state show bump structures with peaks at $r \sim 4$ fm and $r \sim 5$ fm, respectively, and have a long tail up to $r \sim 15$ fm.

It is instructive to study the single α-particle orbits (eigenfunctions) and occupation numbers (eigenvalues) of the one-body density matrix in eq. (20). The results of the diagonalization of the latter are shown in table 2 together with the occupation probability defined as the occupation number divided by the number of α particles. As for the ground state, the occupation probabilities spread out over S, D and G waves, but they are concentrated to the first orbits, S_1, D_1 and G_1 orbits, respectively, where L_k denotes the k-th orbit for the L-wave. The occupation probabilities are about 30% for all orbits. This result is expected from the fact that the ground-state wave function is of nuclear $SU(3)$-like character, $SU(3)[f](\lambda\mu)_{J^\pi} = [444](04)_{0^+}$ with quanta $Q = 8$, where the $SU(3)$ bases with $Q < 8$ correspond to the Pauli-forbidden states [24]. Since the $SU(3)[444](04)_{0^+}$ state is the eigenfunction of the 3α RGM norm kernel, it can be regarded as the 3α boson

Table 2. Occupation numbers of the k-th α orbits with S, D and G waves for the 0^+ and 2^+ states of ^{12}C obtained by diagonalizing the one-body density matrix in eq. (20). The values in parenthesis denote the occupation probabilities.

J^π	k	S	D	G
0_1^+	1	1.05 (35.0%)	1.06 (35.3%)	0.82 (27.3%)
	2	0.01 (0.3%)	0.01 (0.0%)	0.00 (0.0%)
	3	0.00 (0.0%)	0.01 (0.0%)	0.00 (0.0%)
	...	...	...	...
	total	1.07 (35.6%)	1.07 (35.6%)	0.82 (27.3%)
0_2^+	1	2.16 (72.0%)	0.19 (6.3%)	0.08 (2.7%)
	2	0.20 (6.7%)	0.06 (2.0%)	0.06 (2.0%)
	3	0.02 (0.7%)	0.02 (0.7%)	0.01 (0.3%)
	...	...	...	...
	total	2.38 (79.3%)	0.29 (1.0%)	0.16 (5.3%)
2_1^+	1	0.25 (8.5%)	1.69 (56.2%)	1.00 (33.3%)
	2	0.00 (0.0%)	0.02 (0.7%)	0.00 (0.0%)
	3	0.00 (0.0%)	0.00 (0.0%)	0.00 (0.0%)
	...	...	...	...
	total	0.26 (8.7%)	1.71 (57.0%)	1.00 (33.3%)
2_2^+	1	0.31 (10.3%)	2.50 (83.3%)	0.05 (1.7%)
	2	0.02 (0.7%)	0.03 (1.0%)	0.00 (0.0%)
	3	0.00 (0.0%)	0.01 (0.3%)	0.00 (0.0%)
	...	...	...	...
	total	0.33 (11.0%)	2.56 (85.3%)	0.06 (2.0%)

wave function with $Q = 8$. The state is described as

$$|[444](04)\rangle_{0^+} = \sum_{n\ell NL} a_{nlNL}|(n\ell)(NL)\rangle,$$
$$= \sqrt{\frac{64}{225}}|2s2S\rangle - \sqrt{\frac{80}{225}}|1d1D)\rangle + \sqrt{\frac{81}{225}}|0g0G\rangle, \quad (39)$$

where $|(n\ell)(NL)\rangle$ presents the basis function $|u_{n\ell}(\boldsymbol{r}_{2\alpha})u_{NL}(\boldsymbol{r}_{\alpha\text{-}2\alpha})\rangle$ with $2n + \ell + 2N + L = 8$, and $u_{n\ell}$ (u_{NL}) denotes the harmonic-oscillator wave function with the number of nodes n (N) and orbital angular momentum ℓ (L) referring to the coordinate vector $\boldsymbol{r}_{2\alpha}$ ($\boldsymbol{r}_{\alpha\text{-}2\alpha}$) between 2α clusters (between the center of mass for the 2α clusters and the third α cluster). Let us define L_α as the orbital angular momentum of a single-α orbit. Then, L in eq. (39) corresponds to L_α, because L_α is defined as the orbital angular momentum with respect to $\boldsymbol{r}_\alpha^{(\mathrm{cm})}$, coordinate vector of the α particle measured from the center-of-mass coordinate of ^{12}C (see eq. (10)), which is parallel to $\boldsymbol{r}_{\alpha\text{-}2\alpha}$ ($\boldsymbol{r}_\alpha^{(\mathrm{cm})} = \frac{2}{3}\boldsymbol{r}_{\alpha\text{-}2\alpha}$). From the definition of the one-body density matrix in eq. (20), the single-α orbits and occupation probabilities for the $SU(3)$ state in eq. (39) are given as follows: $64/255 \sim 28\%$ for the S orbit, $80/225 \sim 36\%$ for the D orbit, and $81/225 \sim 36\%$ for the G orbit. Thus, we can understand the reason why the S_1, D_1 and G_1 orbits in table 2 have about 30% occupation probabilities each.

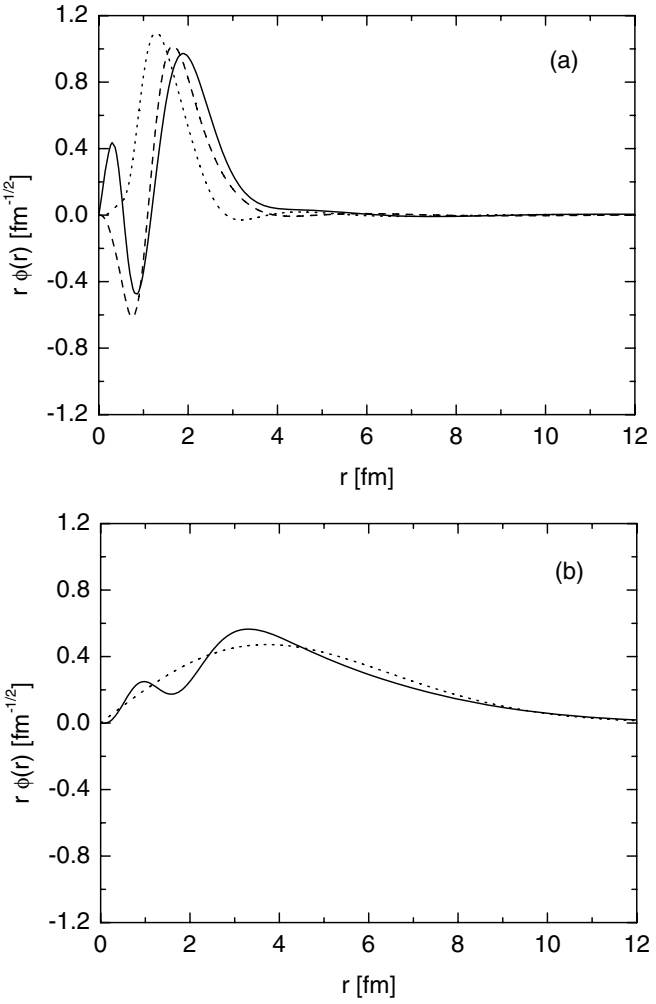

Fig. 4. Radial parts of the single-α orbits, (a) S_1 (solid line), D_1 (dashed line) and G_1 (dotted line), in the 0_1^+ state, and (b) the S_1 (solid line) orbit in the 0_2^+ state and S-wave Gaussian function (dotted line), $r\varphi_{0s}$, with the size parameter $a = 0.038$ fm^{-2} (see text). Note that all of the radial parts in figures are multiplied by r.

Figure 4(a) demonstrates the radial parts for the S_1, D_1 and G_1 orbits, the number of nodes of which is two, one and zero, respectively. Reflecting the $SU(3)$ character, the radial behaviors of the three orbits are similar to those of the harmonic-oscillator wave functions (u_{NL}) with $Q = 4$, u_{02}, u_{21} and u_{40}, respectively, where N (L) denotes the number of nodes (orbital angular momentum). We see that the radial parts of the single α-particle orbits oscillate strongly in the inside region ($r < 4$ fm). This is due to the important Pauli-blocking effect for the ground state with the compact shell-model–like structure. The large oscillation can also be seen in the reduced width amplitude of the $\alpha + {}^8\mathrm{Be}(0^+)$ channel for the ground state shown in fig. 5.

Concerning the 0_2^+ state, the occupation probabilities are shown in table 2. We see a strong concentration on a single orbit: the occupation probability of the S_1 orbit is largest, amounting to about 70%, and those for other orbits are very small. This means that each of the three α particles in the 0_2^+ state is in the S_1 orbit with occupation probability as large as about 70%. The radial behavior of the S_1 orbit is illustrated with the solid line in fig. 4(b). We see no nodal behavior but small oscillations in the inner region ($r < 4$ fm) and a long tail up to $r \sim 10$ fm. For reference, the radial behavior of the S-wave Gaussian function, $\varphi_{0s}(r) = N_{0s}(a)\exp(-ar^2)$, is drawn with the dashed line in fig. 4(b), where the size parameter a is chosen to be 0.038 fm^{-2}, and $N_{0s}(a)$ denotes the normalization factor. The radial behavior of the S_1 orbit is similar to that of the S-wave Gaussian function, in particular, in the outer region ($r > 4$ fm), whereas a slight oscillation of the former around the latter can be seen in the inner region ($r < 4$ fm).

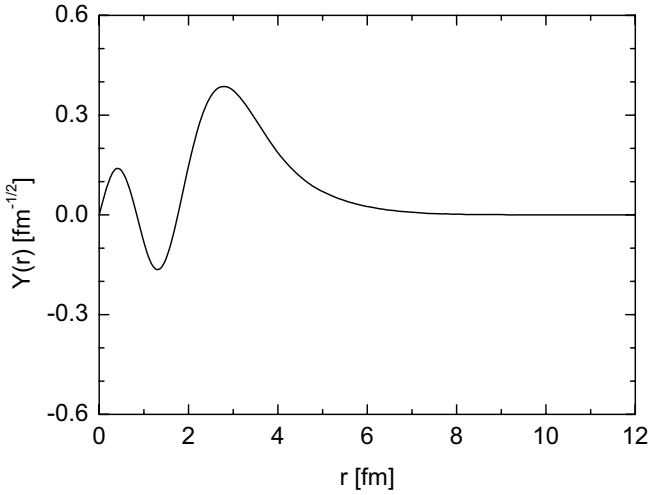

Fig. 5. Reduced width amplitude of the $\alpha + {}^8\mathrm{Be}(0^+)$ channel for the 0_1^+ state.

The small oscillation of the S_1 orbit in the inner region can also be seen in the reduced width amplitude of the 0_2^+ state for the $\alpha + {}^8\mathrm{Be}(0^+)$ channel in fig. 6(a). In order to study the origin of the small oscillation, we show in fig. 6(b) the results of the reduced width amplitudes of the 0_2^+ state for the $\alpha + {}^8\mathrm{Be}(0^+)$ channel, fixing the distance between the 2α clusters in ^{8}Be to $r_{\alpha\alpha} = 0.5, 2.5, 4.5$ and 6.5 fm. In the case of $r_{\alpha\alpha} < 4$ fm, we see the nodal behavior with the large oscillation in the inner region, coming from the strong Pauli-blocking effect among the 3α clusters, while the nodal behavior is disappearing and the oscillations are getting weaker for the larger $r_{\alpha\alpha}$ (≥ 4 fm), reflecting the weaker Pauli-blocking effect. Thus, the small oscillations in the radial behavior of the S_1 orbit is evidence for the weak Pauli-blocking effect for the 0_2^+ state with the dilute structure.

The momentum distributions of the α particles, $\rho(k)$ and $k^2 \times \rho(k)$, are shown for the 0_1^+ and 0_2^+ states in fig. 7. Reflecting the dilute structure of the 0_2^+ state, we see a strong concentration of the momentum distribution in the $k < 1$ fm^{-1} region, and the behavior of $\rho(k)$ is of the δ-function type, similar to the momentum distribution of the dilute neutral atomic condensate states at very low temperature trapped by the external magnetic field [7]. On the other hand, the ground state has higher

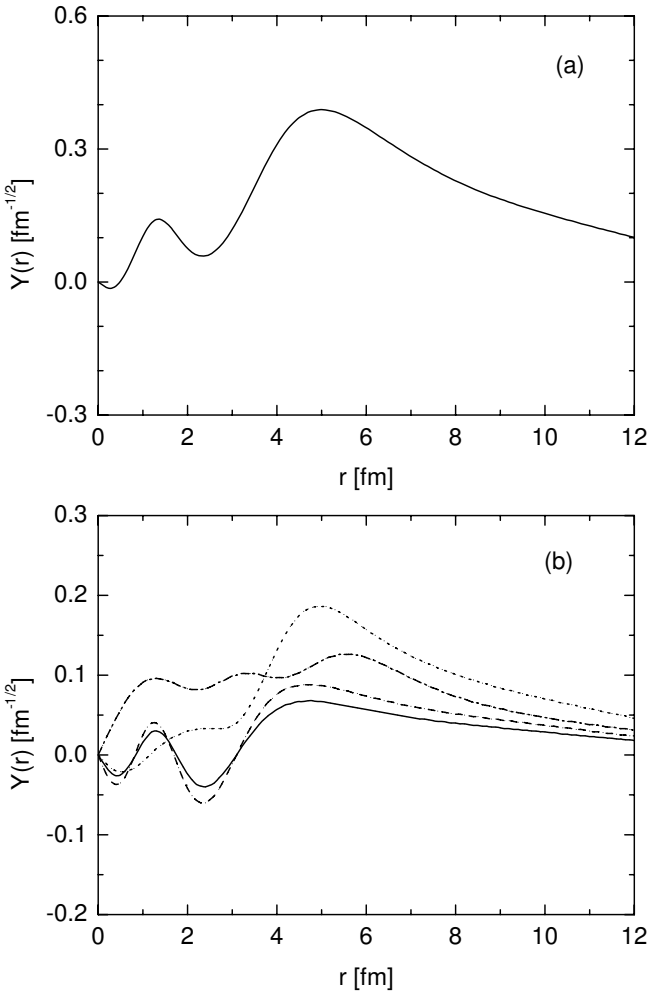

Fig. 6. (a) Reduced width amplitude of the $\alpha + {}^{8}\mathrm{Be}(0^+)$ channel for the 0_2^+ state, and (b) reduced width amplitudes in which the distance between the 2α clusters in ^{8}Be is fixed to $r_{\alpha\alpha} = 0.5, 2.5, 4.5$ and 6.5 fm.

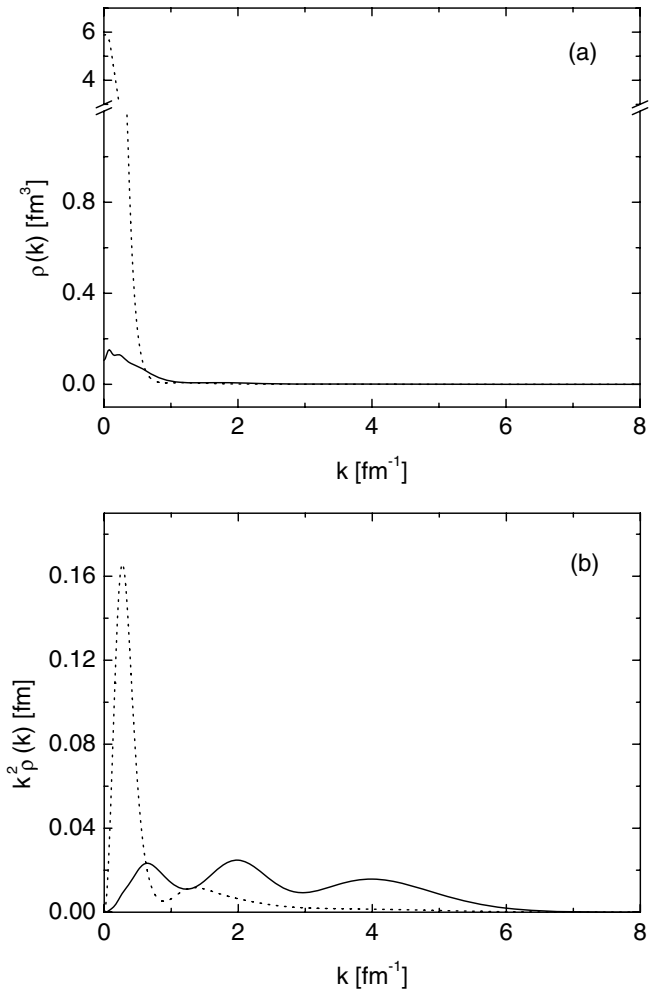

Fig. 7. Momentum distribution of the α particle, (a) $\rho(k)$ and (b) $k^2 \times \rho(k)$, for the 0_1^+ (solid line) and 0_2^+ (dotted line) states.

momentum component up to $k \sim 6$ fm^{-1} as seen from the behavior of $k^2 \times \rho(k)$ reflecting the compact structure. The above results for the radial behavior of the S_1 orbit, occupation probability and momentum distribution for the 0_2^+ state leads us to conclude that this state is similar to an ideal dilute 3α condensate with as much as about 70% occupation probability.

Let us make some remarks on the calculated energy ($E_{3\alpha} = 0.85$ MeV) and wave function of the 0_2^+ state. They were evaluated under the bound-state approximation in the present study (see sect. 2). The quite small experimental width for 0_2^+ ($\Gamma = 8.5$ eV) [27] means that the bound-state approximation is very good to describe the wave function. The complex-scaling method [28] is powerful to search for resonant states and calculate the exact energies and widths, and is applied easily to the 3α system by slightly modifying the present framework. The detailed framework is skipped here and referred to ref. [28]. In the present study, we investigated the energy of the 0_2^+ state with the complex-scaling method. It was found that a resonant state, corresponding to the 0_2^+ state, appears at $E_{3\alpha} = 0.85$ MeV with a width less than the numerical uncertainty (~ 100 keV in the present calculation). The results confirm that the bound-state approximation is good to describe the 0_2^+ resonant state.

It is interesting to compare our results with those given by Matsumura *et al.* [17], who used the normalized spectroscopic amplitude to obtain the bosonic quantities such as the single-α orbits and occupation probabilities for the 0_2^+ state in place of the 3α boson wave function. According to their results, the occupation probability of the S_1 orbit ($0S$ orbit in ref. [17]) for the 0_2^+ state is about 70%, the value of which is quite similar to ours in table 2. However, the radial behavior of the S_1 orbit for the 0_2^+ state as well as the one of the 0_1^+ state given by Matsumura *et al.* are quite different from our results, and seem unnatural. For example, the S_1 orbit for the 0_2^+ state has as much as 6–8 nodes and shows a behavior similar to that for the 0_1^+ state, in spite of the fact that the 0_2^+ state has a dilute 3α condensate structure (see fig. 6 in ref. [17]). In addition, the G orbit for 0_1^+ state has a prominent peak at $r \sim 13$ fm, although the state has a shell-model–like compact

structure. Also the radial behavior of the single-α orbits given in ref. [17] is hard to understand. This may be due to the fact that those authors used the normalized spectroscopic amplitude in place of the 3α boson wave function.

3.2 2_1^+ and 2_2^+ states

The 2_1^+ state at $E_{3\alpha}^{\rm exp} = -2.83$ MeV ($E_x = 4.44$ MeV) belongs to the rotational band of the ground state starting from the 0_1^+ state at $E_{3\alpha}^{\rm exp} = -7.27$ MeV. The calculated energy and nuclear radius for 2_1^+ in the present study are shown in table 1: $E_{3\alpha} = -5.28$ MeV and 2.45 fm, respectively. The nuclear radius is almost the same as the one for the ground state, although the calculated excitation energy is underestimated in comparison with the experimental one, in line with what is discussed in other papers with the microscopic or semi-microscopic 3α cluster model [4,18–20,23].

The occupation probabilities of the single-α orbits for 2_1^+ are demonstrated in table 2. The occupation numbers are concentrated to the first D_1 and G_1 orbits with about 50%. Comparing with those for the 0_1^+ state, we notice the smallness of the occupation number for the S_1 orbit. This feature can be understood from the fact that the 2_1^+ state is of the $SU(3)[f](\lambda\mu)_J = [444](04)_{2^+}$ type with $Q = 8$. The $SU(3)$ state is described as

$$\begin{aligned}|[444](04)\rangle_{2^+} = &\sqrt{0.07111}|1d2S\rangle + \sqrt{0.07111}|2s1D\rangle \\ &-\sqrt{0.43900}|1d1D\rangle - \sqrt{0.00735}|0g1D\rangle \\ &-\sqrt{0.00735}|1d0G\rangle + \sqrt{0.40408}|0g0G\rangle. \end{aligned} \quad (40)$$

From the definition of the one-body density matrix in eq. (20), the occupation probabilities for the $SU(3)$ state in eq. (40) are given as 0.07111 for the S orbit, $0.07111 + 0.43900 + 0.00735 = 0.51746$ for the D orbit, and $0.00735 + 0.40408 = 0.41143$ for the G orbit. Reflecting the character of the $SU(3)$ structure, the occupation probability for the S_1 orbit in table 2 is as small as 8.5%. The radial behavior of the single-α orbits, S_1, D_1 and G_1 ones, is shown in fig. 8(a). They are similar to those for the 0_1^+ state shown in fig. 4(a).

The structure study of ^{12}C based on the 3α-condensate–type wave function [15] indicated that the 2_2^+ state at $E_{3\alpha}^{\rm exp} = 2.6 \pm 0.3$ MeV with the width of $\Gamma = 1.0 \pm 0.3$ MeV [14] has a structure similar to the 0_2^+ state at $E_{3\alpha} = 0.38$ MeV with the dilute 3α condensation [15]. The conclusion stems from the result that the 2_2^+ state has a large overlap with the single condensate wave function of a 3α gas-like structure, the squared value of which amounts to about 88%. Thus, it is interesting to study the structure of the 2_2^+ state in the present framework. Since the 2_2^+ state is a resonant state with non-negligible width, a continuum treatment is requested to estimate exactly the resonant energy and width.

In order to study the resonant properties of the 2_2^+ state, we take the complex-scaling method [28], which can be applied easily to the present 3α system by slightly modifying the framework given in sect. 2. The method

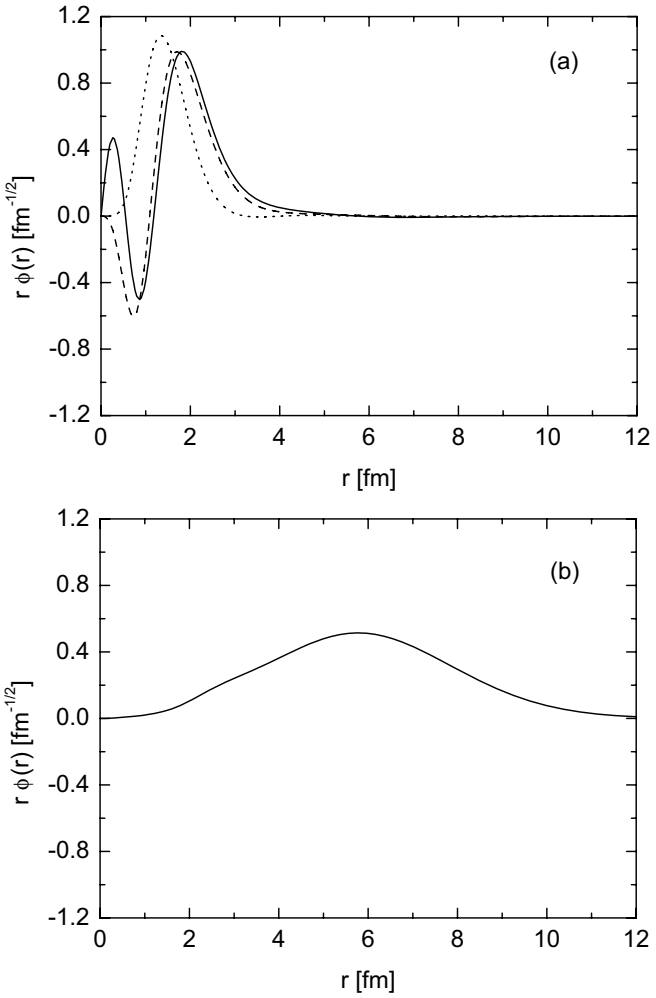

Fig. 8. Radial parts of the single-α orbits, (a) S_1 (solid line), D_1 (dashed line) and G_1 (dotted line), in the 2_1^+ state, and (b) the D_1 (solid line) orbit in the 2_2^+ state. Note that all the radial parts in the two panels are multiplied by r.

is powerful to evaluate not only the resonant energy and width but also the nuclear radius. The details are again skipped here and we refer to ref. [28]. The calculated results are as follows: 1) the 2_2^+ resonant state is located at $E_{3\alpha} = 2.3$ MeV with $\Gamma = 1.0$ MeV, which is in good agreement with the experimental data [14], and 2) the calculated nuclear radius is 4.3 fm, almost the same as that of the 0_2^+ state. Thus, the 2_2^+ state has a dilute 3α structure.

It is interesting to study the single-α orbits and occupation probabilities in the 2_2^+ state. For this purpose, we need to have the wave function of the 2_2^+ state. Since the calculated width is not so large in comparison with the resonance energy, the bound-state approximation is rather good to describe the resonant wave function. The bound-state approximation of the wave function is obtained within the framework of sect. 2, although the wave function gives a large nuclear radius, about 6 fm (see table 1). Table 2 illustrates the occupation probabilities of the single-α orbits (S, D and G waves) for the 2_2^+ state. We see that the occupation probability concentrates on only one

orbit, the D_1 orbit, with occupancy as large as 83%, and the radial behavior of the orbit is likely to be of the D-wave Gaussian-function–type with a long tail (see fig. 8(b)), reflecting a dilute structure. These characteristics are quite similar to those for the 0_2^+ state. Thus, we conclude that the 2_2^+ state belongs to the 3α condensate structure.

According to the results in ref. [15], it was found that the 2_2^+ state has a dominant S-wave between 2α particles and a D-wave between the center of mass of the 2α particles and the third α,

$$\Phi(2_2^+) \sim |u_{\ell=0}(\boldsymbol{r}_{2\alpha})U_{L=2}(\boldsymbol{r}_{\alpha\text{-}2\alpha})\rangle. \tag{41}$$

This interpretation is consistent with the present result. The reason is as the follows. From the definition of the single-α density matrix in eq. (20), the single-α density of the 2_2^+ state is presented as

$$\rho(\boldsymbol{r},\boldsymbol{r}') = 3 \times \langle \Phi(2_2^+)|\delta(\boldsymbol{r}_1^{(\mathrm{cm})} - \boldsymbol{r}')\rangle\langle\delta(\boldsymbol{r}_1^{(\mathrm{cm})} - \boldsymbol{r})|\Phi(2_2^+)\rangle, \tag{42}$$

$$\sim 3 \times N_{2\alpha} \times U_{L=2}(\boldsymbol{r})U_{L=2}{}^*(\boldsymbol{r}'), \tag{43}$$

where $N_{2\alpha} = \int \mathrm{d}\boldsymbol{r}_{2\alpha} u_0{}^*(\boldsymbol{r}_{2\alpha})u_0(\boldsymbol{r}_{2\alpha}) \sim 1$. Thus, the 2_2^+-state wave function, eq. (41), has a dominant occupation probability of the D orbit, $U_{L=2}$. The results are in good agreement with the present study.

3.3 3_1^- state

The 3^- state at $E_{3\alpha}^{\mathrm{exp}} = 2.37$ MeV is an interesting one from the point of view of the dilute α condensation. If the state is a condensate with all of the 3α particles in the P orbit, there is the possibility of a superfuid with vortex lines, similar to the rotating dilute atomic condensate at very low temperature [7]. Thus, it is an intriguing problem to study the structure in the present framework.

The calculated energy of the 3^- state is in good agreement with the experimental data (see table 1). The very small width ($\Gamma^{\mathrm{exp}} = 3.4$ keV) [27] indicates that the bound-state approximation is very good to describe the state. In fact, we checked it theoretically with the complex-scaling method, and found that the calculated resonant energy (width) is almost the same as the one with the bound-state approximation (less than 100 keV, which is the numerical uncertainty in the present calculation). Thus, we use the 3^- wave function under the bound-state approximation to study the characteristics of the state.

The calculated nuclear radius for the 3^- state is 2.95 fm, the value of which is larger than that for the ground state (0_1^+), while it is smaller than that for the 0_2^+ state (see table 1). This suggests that the structure of the 3^- state is intermediate between the shell-model–like compact structure (0_1^+) and the dilute 3α structure (0_2^+). The occupation probabilities of the single-α orbits for the 3^- state are shown in table 3: 44.7% for the P_1 orbit and 27.9% for the F_1 orbit. Although the concentration of the single orbit P_1 amounts to about 50%, the radial behavior of the single-α orbit in fig. 9 has two nodes in the inner region. However, the amplitude of the inner oscillations is significantly smaller than that for the ground state in fig. 3(a). The small oscillations indicate the weak Pauli-blocking effect, and thus, we can see the precursor of the 3α condensate state, although the 3^- state is not an ideal rotating dilute 3α condensate.

Table 3. Occupation numbers of the k-th α orbits with P and F waves for the 3^- and 1^- states of ^{12}C obtained by diagonalizing the one-body density matrix in eq. (20). The values in parenthesis denote the occupation probabilities.

J^π	k	P	F
3_1^-	1	1.34 (44.7%)	0.84 (27.9%)
	2	0.12 (4.0%)	0.23 (7.5%)
	3	0.06 (1.9%)	0.02 (0.8%)
	...	...	...
	total	1.54 (51.4%)	1.09 (36.4%)
1_1^-	1	1.06 (35.3%)	0.47 (15.8%)
	2	0.53 (17.8%)	0.26 (8.6%)
	3	0.08 (2.6%)	0.08 (2.6%)
	...	...	...
	total	1.75 (58.5%)	0.84 (28.1%)

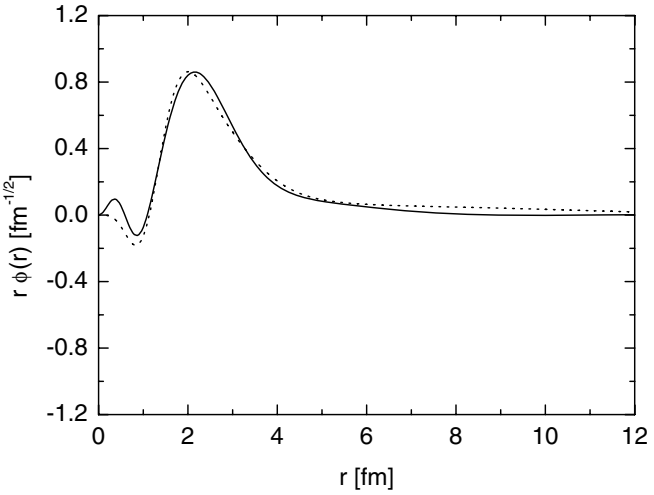

Fig. 9. Radial parts of the single-α orbits, P_1 (solid line) and F_1 (dotted line), in the 3_1^- state. Note that all the radial parts in the figure are multiplied by r.

3.4 1_1^- state

The experimental width of the 1_1^- state at $E_{3\alpha}^{\mathrm{exp}} = 3.57$ MeV is as small as $\Gamma = 315$ keV [27]. This means that the bound-state approximation is good to describe the state. In fact, the calculated energy of the 1_1^- state under the bound-state approximation is $E_{3\alpha} = 3.11$ MeV, which is quite similar to that with the complex-scaling method ($E_{3\alpha} = 3.1$ MeV and $\Gamma = 0.1$ MeV) and in good agreement with the experimental value.

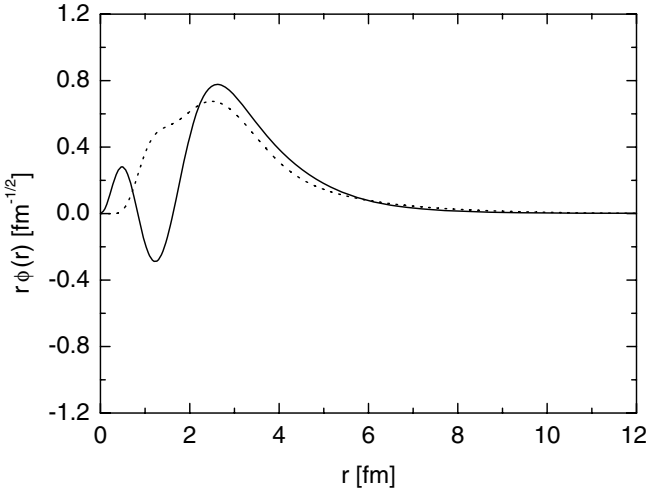

Fig. 10. Radial parts of the single-α orbits, P_1 (solid line) and F_1 (dotted line), in the 1^-_1 state. Note that all the radial parts in the figure are multiplied by r.

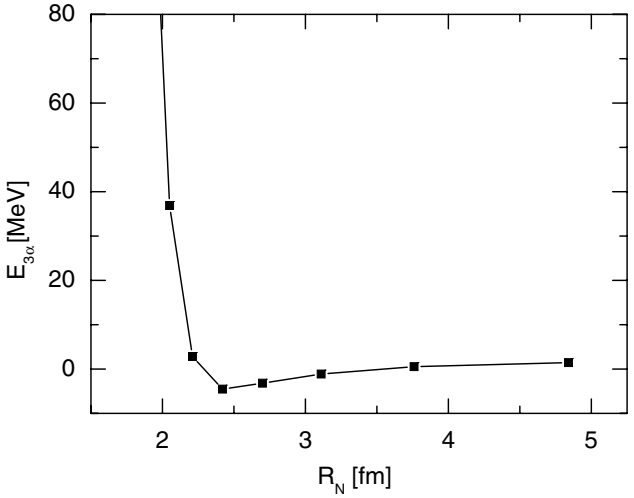

Fig. 11. Dependence of the energy of the ^{12}C(0^+) state, measured from the 3α threshold, on its nuclear radius.

The calculated nuclear radius, 3.32 fm, is larger than that of the ground state (2.44 fm) and the 3^-_1 state (2.95 fm) but is smaller than that of the 0^+_2 one (4.3 fm). The occupation probabilities of the α particles in the 1^-_1 state are shown in table 3: 35% for the P_1 orbit and 16% for the F_1 orbit. Thus, there is no concentration of the occupation probability to a single orbit like the 0^+_2 and 2^+_2 states. Since the α particles in the 1^-_1 state are distributed over in several orbits, the state is not of the dilute α condensate type. Figure 10 shows the radial behavior of the P_1 and F_1 orbits in the 1^-_1 state. The P_1 orbit has two nodes in the inner region, the behavior of which is rather similar to the $2P$ harmonic-oscillator wave function. However, the F_1 orbit has a F-wave Gaussian-type behavior. (Exactly speaking, the orbit has one node at the vicinity of the origin, which cannot be seen in fig. 10.) Also we see the oscillatory behavior of the F_1 orbit for $0 < r < 2$ fm, similar to the one of the S_1 orbit in the 0^+_2 state in fig. 4(b). These interesting behaviors of the F_1 orbit indicate some signal of the dilute α condensation, reflecting the relatively large nuclear radius (3.32 fm) for the 1^-_1 state.

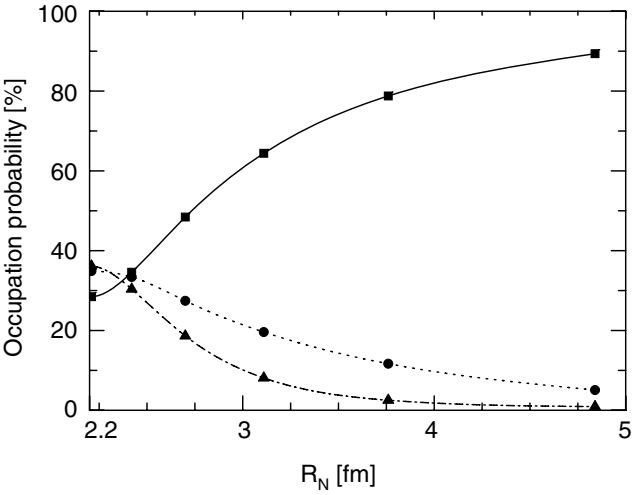

Fig. 12. Dependence of the occupation probabilities of the single-α orbits (S_1, D_1 and D_1 orbits) in the ^{12}C(0^+) state on its nuclear radius. The solid (dotted and dot-dashed) line corresponds to the S_1 orbit (D_1 and G_1 orbits, respectively).

3.5 Structure change of the 0^+ state with nuclear radius

In sect. 3.1, we found that the 0^+_2 state has a dilute 3α structure characterized by the nuclear radius as large as about 4.3 fm, in which the α particle occupies the single orbit (S_1) with about 70% probability, and the radial behavior of the S_1 orbit is similar to the S-wave Gaussian wave function with a very long tail. On the other hand, the 0^+_1 state has a compact structure with a nuclear radius of 2.44 fm, where the occupation probabilities of the α particles spread out over the S, D and G orbits, amounting to about 30%, each. The feature is much in contrast with that of the 0^+_2 state. The nuclear radius or density of ^{12}C seems to have a close relation with making the compact structure and the dilute 3α structure in the ^{12}C 0^+ state. Thus, it is very interesting to see the structure change of the 0^+ state of ^{12}C by taking the nuclear radius (or density) as parameter.

The dependence of the occupation probabilities and radial behaviors of the single α-particle orbits in the 0^+ state on its nuclear radius is investigated with the use of the simple framework given in the latter part of sect. 2.2 (see eqs. (36), (37) and (38)). According to the results of the 3α OCM calculation (see sect. 3.1), the ground state (0^+_1) and second 0^+_2 states of ^{12}C have the equilateral-triangle configuration of the 3α clusters. In addition, it is found that the single angular-momentum channel calculation with $c = (\ell L)_J = (00)_0$ gives a good approximation to the results of the full coupled-channel calculation. Thus, only

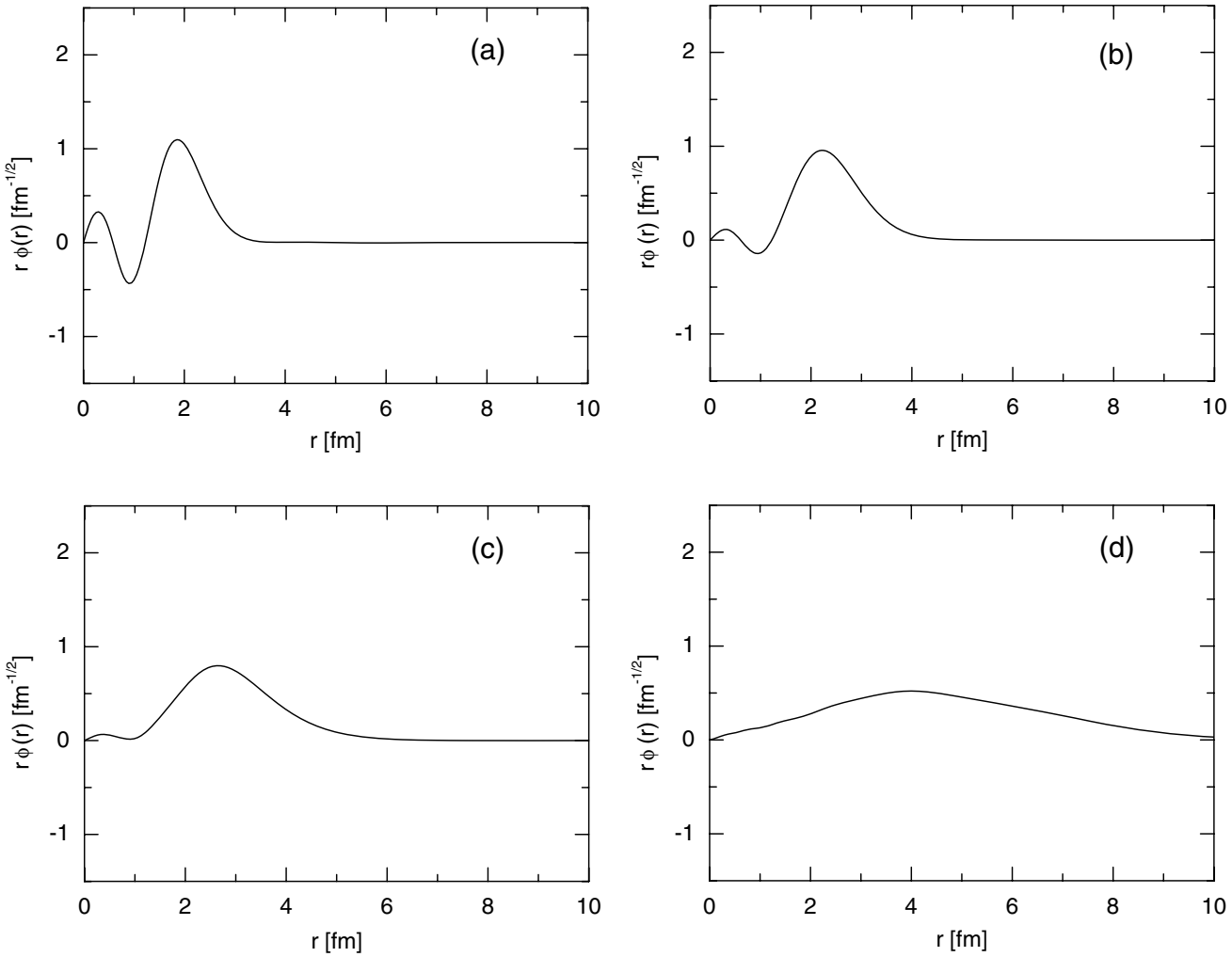

Fig. 13. Radial behaviors of the S_1 orbit in the ^{12}C(0^+) state with (a) $R_N = 2.42$ fm, (b) $R_N = 2.70$ fm, (c) $R_N = 3.11$ fm, and (d) $R_N = 4.84$ fm, where R_N denotes the nuclear radius of the ^{12}C(0^+) state.

the single angular-momentum channel $c = (\ell L)_J = (00)_0$ is taken in the present calculation, and the equilateral-triangle configuration is assumed for the Pauli-principle–respecting 3α OCM basis wave function (eq. (37)). The latter can be realized easily by putting the condition $\nu = \mu$ in eq. (37). We have checked it by calculating the rms radii $\sqrt{\langle r^2_{\alpha\alpha}\rangle}$ and $\sqrt{\langle r^2_{\alpha\text{-}2\alpha}\rangle}$ defined in eqs. (15) and (16).

Figure 11 shows the dependence of the energy of ^{12}C measured from the 3α threshold on the nuclear radius R_N, 2.20 fm $\leq R_N \leq$ 4.86 fm, corresponding to a nuclear density $0.15 \leq \rho/\rho_0 \leq 1.6$ (ρ_0 denotes the normal density). The energy minimum point appears around $R_N \sim 2.4$ fm, corresponding to the normal density region. We see the strong repulsion in the region of $R_N < 2.2$ fm, due to the kinetic-energy effect and Pauli-blocking effect, while the almost flat region appears at $R_N > 4$ fm and the energy is positive and small, less than 1 MeV with respect to the 3α threshold.

The occupation probabilities of the single-α orbits (S_1, D_1, and G_1 orbits) are shown in fig. 12 with respect to the nuclear radius, where L_k denotes the k-th orbit for the L-wave. In the region of $R_N = 2.2$–2.4 fm (normal density region), the occupation probabilities of the α particles spread out over the S, D and G orbits, amounting to about 30% each. This feature is almost the same as that of the 0^+_1 state obtained by the 3α OCM calculation, the nuclear radius of which is 2.43 fm (see sect. 3.1). Figure 13 shows the radial behavior of the single-α orbit, S_1, with respect to the nuclear radius. The S_1 orbit at $R_N \sim 2.42$ fm (fig. 13(a)) has two nodes and the radial behavior is of the $2S$ harmonic-oscillator wave function (howf) type, the result of which is almost the same as that of the 0^+_1 state obtained by the 3α OCM calculation (see fig. 4(a)). Thus, the wave function with $R_N \sim 2.4$ fm has the $SU(3)[f](\lambda\nu) = [444](04)$ character (see eq. (39)).

Increasing the nuclear radius from $R_N = 2.42$ fm, the occupation probability of the single-α orbits concentrates gradually on a single orbit (S_1), and it amounts to be about 90% at $R_N = 4.84$ fm ($\rho/\rho_0 = 0.14$) in the present calculation (see fig. 12). The radial behaviors of the S_1

orbit with $R_N = 2.42, 2.70, 3.11$ and 4.84 fm are demonstrated in figs. 13(a), (b), (c) and (d), respectively. We can see that increasing the nuclear radius, the internal oscillation observed in the S_1 orbit with $R_N = 2.42$ fm is gradually disappearing and, finally, the $2S$-type radial behavior transits to the zero-node long-ranged S-wave type (Gaussian) with the occupation probability of about 90%, approaching an ideal dilute α condensate. The reason why only the S-wave survives in the case of increasing the nuclear radius is due to the fact that the centrifugal barrier is not at work for the S-wave α orbit. The S-wave α particles, thus, can move in a nucleus with a given large nuclear radius, although they are confined by the Coulomb potential barrier produced self-consistently [12]. According to the results of the 3α OCM calculation (see sect. 3.1), the α particle in the 0_2^+ state ($R_N = 4.3$ fm) is occupied in the single orbit (S_1) with about 70% probability, the radial behavior of which is similar to the S-wave Gaussian wave function with a very long tail. These results are consistent with those in figs. 12 and 13.

4 Summary

In this work we have investigated the bosonic properties such as single-α particle orbits and occupation numbers in the $J^\pi = 0^+, 2^+, 1^-$, and 3^- states of ^{12}C around the 3α threshold within the framework of the 3α OCM (orthogonality condition model). The 3α OCM equation is based on the equation of motion for the $N\alpha$ bosons derived from the microscopic $N\alpha$ cluster model theory. The experimental energy spectra for 0_1^+, 0_2^+, 2_2^+, 1_1^-, and 3_1^- are reproduced well with the 3α OCM.

The main results to be emphasized here are as follows.

1) The 0_2^+ state at $E_{3\alpha}^{\rm exp} = 0.38$ MeV has a dilute 3α structure characterized by the nuclear radius as large as about 4.3 fm. The analysis of the single-α orbits and occupation probabilities for the dilute state shows that the α particle is occupied in a single orbit (S_1) with about 70% probability, and the radial behavior of the S_1 orbit is similar to the S-wave Gaussian wave function with a very long tail. The momentum distribution of the α particle illustrates the δ-function–like behavior, similar to the momentum distribution of dilute neutral atomic condensate states at very low temperature, a feature which eventually can be measured experimentally. These results give more theoretical evidence that the 0_2^+ state is a dilute 3α condensate. On the other hand, the 0_1^+ state has a compact structure with a nuclear radius of 2.44 fm. The occupation probabilities of the α particles spread out over the S, D and G orbits, amounting to about 30%, each, the results of which comes from the fact that the 0_1^+ state is characterized by the nuclear $SU(3)$ wave function, $[f](\lambda\mu) = [444](04)$. The feature is much in contrast with that of the 0_2^+ state.

2) In order to understand further the characteristic structure of the two 0^+ states, we have studied the single-α orbital behavior in the ^{12}C(0^+) state by taking the nuclear radius R_N (or density ρ/ρ_0) as parameter, $2.42 \leq R_N \leq 4.84$ fm ($0.15 \leq \rho/\rho_0 \leq 1.2$), where ρ_0 denotes the normal density). We found that the single-α orbits in the ^{12}C(0^+) state are smoothly changed with the nuclear radius R_N, and their behavior is classified into the following three types, depending on the value of R_N: i) at $R_N \sim 2.4$ fm ($\rho/\rho_0 \sim 1$), we have two-nodal S orbit ($2S$), one-nodal D orbit ($1D$) and zero-nodal G orbit ($0G$) with about 30% occupation probability, each, characterized by a nuclear $SU(3)$ wave function, ii) increasing the nuclear radius from $R_N \sim 2.4$ fm, the occupation probability of the single-α orbits concentrates gradually on a single S orbit, in which the two-nodal behavior is disappearing, and then, iii) at $R_N \sim 4$ fm ($\rho/\rho_0 \sim 0.2$), there appears a dominant zero-nodal Gaussian ($0S$-type) orbit with a very long tail, the radial behavior of which is similar to that of the 0_2^+ state in ^{12}C as mentioned above. The structure change is caused mainly by the Pauli-blocking effect, the strength of which depends dominantly on the nuclear radius R_N in the present framework.

3) The structure of the 2_2^+ state at $E_{3\alpha}^{\rm exp} = 2.6 \pm 0.3$ MeV with $\Gamma = 1.0 \pm 0.3$ MeV was studied with the present 3α OCM and the complex-scaling method. We found that the 2_2^+ resonant state appears at $E_{3\alpha} = 2.3$ MeV with $\Gamma = 1.0$ MeV, in agreement with the experimental data, and the calculated nuclear radius is 4.3 fm, similar to that of the 0_2^+ state. The 2_2^+ wave function obtained with the 3α OCM was used to study the bosonic properties of the state. It was found that the occupation probability of the α particle concentrates only on the D_1 orbit, amounting to be as large as about 80%, and the radial behavior is of the D-wave Gaussian type with a long tail. The characteristics of the boson properties in 2_2^+ is quite similar to those in 0_2^+ at $E_{3\alpha}^{\rm exp} = 0.38$ MeV. Thus, the 2_2^+ state has an excited dilute-3α-condensate–like structure. On the other hand, the 2_1^+ state has a compact structure with the nuclear radius, 2.44 fm, like the ground state. The occupation probabilities of the α particles spread out over the D and G orbits, amounting to about 56% and 33%, respectively, reflecting the $SU(3)$ character of the 2_1^+ state.

4) We investigated the α bosonic properties of the negative parity states, 1_1^- at $E_{3\alpha}^{\rm exp} = 3.57$ MeV and 3_1^- at $E_{3\alpha}^{\rm exp} = 2.37$ MeV. Their nuclear radii are 3.32 and 2.95 fm, respectively, which are larger than that of the ground state (0_1^+) but smaller than that of 0_2^+. The calculated occupation probabilities of the α particles in those states show that there is no concentration on a single-α orbit like in the 0_2^+ and 2_2^+ states. The results indicates that the 1^- and 3_1^- states are not of the dilute 3α condensate. The radial behavior of the P- and F-wave single-α orbits, however, suggests that small components of the 3α condensation exist even in the negative-parity states, which is reflected by their relatively large nuclear radii.

We acknowledge helpful discussions with H. Horiuchi, K. Ikeda, G. Röpke, A. Tohsaki, Y. Suzuki, and Y. Funaki.

References

1. K. Wildermuth, Y.C. Tang, *A Unified Theory of the Nucleus* (Vieweg, Braunschweig, Germany, 1977).
2. D.M. Brink, in *Many-Body Description of Nuclear Structure and Reactions*, *Proceedings of the International School of Physics "Enrico Fermi", Course XXXVI*, edited by C. Bloch (Academic Press, New York, 1966).
3. G.F. Bertsch, W. Bertozzi, Nucl. Phys. A **165**, 199 (1971).
4. Y. Fujiwara, H. Horiuchi, K. Ikeda, M. Kamimura, K. Kato, Y. Suzuki, E. Uegaki, Prog. Theor. Phys. Suppl. **68**, 29 (1980).
5. E. Uegaki, S. Okabe, Y. Abe, H. Tanaka, Prog. Theor. Phys. **57**, 1262 (1977); E. Uegaki, Y. Abe, S. Okabe, H. Tanaka, Prog. Theor. Phys. **59**, 1031 (1978); **62**, 1621 (1979).
6. Y. Fukushima, M. Kamimura, *Proceedings of the International Conference on Nuclear Structure, Tokyo, 1977*, edited by T. Marumori, Suppl. J. Phys. Soc. Jpn. **44**, 225 (1978); M. Kamimura, Nucl. Phys. A **351**, 456 (1981).
7. F. Dalfovo, S. Giorgini, L.P. Pitaevskii, S. Stringari, Rev. Mod. Phys. **71**, 463 (1999).
8. G. Röpke, A. Schnell, P. Schuck, P. Nozieres, Phys. Rev. Lett. **80**, 3177 (1998).
9. M. Beyer, S.A. Sofianos, C. Kuhrts, G. Röpke, P. Schuck, Phys. Lett. B **80**, 247 (2000).
10. A. Tohsaki, H. Horiuchi, P. Schuck, G. Röpke, Phys. Rev. Lett. **87**, 192501 (2001).
11. Y. Funaki, H. Horiuchi, A. Tohsaki, P. Schuck, G. Röpke, Prog. Theor. Phys. **108**, 297 (2002).
12. T. Yamada, P. Schuck, Phys. Rev. C **69**, 024309 (2004).
13. L.P. Pitaevskii, Zh. Eksp. Teor. Fiz. **40**, 646 (1961) (Sov. Phys. JETP **13**, 451 (1961)); E.P. Gross, Nuovo Cimento **20**, 454 (1961); J. Math. Phys. **4**, 195 (1963).
14. M. Itoh *et al.*, Nucl. Phys. A **738**, 268 (2004).
15. Y. Funaki, A. Tohsaki, H. Horiuchi, P. Schuck, G. Röpke, Eur. Phys. J. A **24**, 321 (2005), arXiv: nucl-th/0410097.
16. V.I. Kukulin, V.M. Krasnopol'sky, J. Phys. A **10**, 33 (1977); V.I. Kukulin, V.M. Krasnopol'sky, M. Miselkhi, Sov. J. Nucl. Phys. **29**, 421 (1979).
17. H. Matsumura, Y. Suzuki, Nucl. Phys. A **739**, 238 (2004).
18. S. Saito, Prog. Theor. Phys. **40**, 893 (1968); **41**, 705 (1969).
19. H. Horiuchi, Prog. Theor. Phys. **51**, 1266 (1974); **53**, 447 (1975).
20. K. Fukatsu, K. Kato, H. Tanaka, Prog. Theor. Phys. **81**, 738 (1989); K. Fukatsu, K. Kato, Prog. Theor. Phys. **87**, 151 (1992).
21. E.M. Tursunov, D. Baye, P. Descouvemont, Nucl. Phys. A **723**, 365 (2003); P. Descouvemont, C. Daniel, D. Baye, Phys. Rev. C **67**, 044309 (2003).
22. Y. Fujiwara, M. Kohno, Y. Suzuki, Phys. Rev. C **69**, 037002 (2004); Y. Fujiwara, K. Miyagawa, M. Kohno, Y. Suzuki, D. Baye, J.-M. Sparenberg, Phys. Rev. C **70**, 024002 (2004).
23. C. Kurokawa, K. Kato, Nucl. Phys. A **738**, 455 (2004).
24. H. Horiuchi, K. Ikeda, *Cluster Model of the Nucleus*, Int. Rev. Nucl. Phys., Vol. **4** (World Scientific Publishing Co., 1986) p. 1.
25. M. Kamimura, Phys. Rev. A **38**, 621 (1988); H. Kameyama, M. Kamimura, Y. Fukushima, Phys. Rev. C **40**, 974 (1989); E. Hiyama, Y. Kino, M. Kamimura, Prog. Part. Nucl. Phys. **51**, 1 (2003).
26. V.I. Kukulin, V.M. Krasnopol'sky, V.T. Voronchev, P.B. Sazanov, Nucl. Phys. A **417**, 128 (1984).
27. F. Ajzenberg-Selove, Nucl. Phys. A **506**, 1 (1990).
28. A.T. Kruppa, R.G. Lovas, B. Gyarmati, Phys. Rev. C **37**, 383 (1988); M. Homma, T. Myo, K. Kato, Prog. Theor. Phys. **97**, 561 (1996).